

8-30-2011

# Physics-based model and data analysis for the estimation of transverse flowing particles

Michael Thomas

Follow this and additional works at: [https://digitalrepository.unm.edu/ece\\_etds](https://digitalrepository.unm.edu/ece_etds)

---

## Recommended Citation

Thomas, Michael. "Physics-based model and data analysis for the estimation of transverse flowing particles." (2011).  
[https://digitalrepository.unm.edu/ece\\_etds/250](https://digitalrepository.unm.edu/ece_etds/250)

This Thesis is brought to you for free and open access by the Engineering ETDs at UNM Digital Repository. It has been accepted for inclusion in Electrical and Computer Engineering ETDs by an authorized administrator of UNM Digital Repository. For more information, please contact [disc@unm.edu](mailto:disc@unm.edu).

**Michael Thomas**

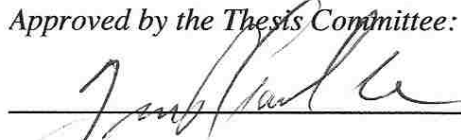
*Candidate*

*Electrical and Computer Engineering*

*Department*

This thesis is approved, and it is acceptable in quality and form for publication:

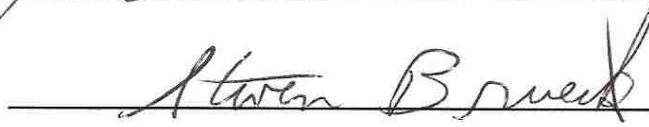
*Approved by the Thesis Committee:*



Dr. Jim Plusquellic  
, Chairperson



Dr. Steven Graves



Dr. Steven Brueck

---

---

---

---

---

---

---

---

---

---

**Iterative Model and Data Analysis for the Estimation of Transverse  
Flowing Particles**

**BY**

**Michael Thomas**

**B.S. Electrical Engineering  
New Mexico State University**

**THESIS**

Submitted in Partial Fulfillment of the  
Requirements for the Degree of

**Master of Science**

**Electrical Engineering**

The University of New Mexico  
Albuquerque, New Mexico

**July, 2011**

## **DEDICATION**

To my family and friends, for your endless support and encouragement, for my completion of this thesis would not have been possible without.

## **ACKNOWLEDGMENTS**

I heartily acknowledge Dr. Jim Plusquellic as my advisor and this committee chair for his guidance and encouragement inside and outside of the classroom. Thank you for your feedback and support over the past several months.

I would also like to thank Dr. Steve Graves for his financial support throughout my graduate career and continual guidance and input regarding my research. In addition I thank Dr. Graves for his participation on my thesis committee.

I thank Mr. Mark Naiver and Dr. Robert Applegate for their technical guidance throughout the duration of this project, and also Dr. Steven Brueck who has graciously offered to serve on this Master's thesis committee.

Finally, I thank my colleagues belonging to both Dr. Plusquellic's and Dr. Grave's research groups for their continual support, input and positive work environment throughout the duration of this project.

**Iterative Model and Data Analysis for the Estimation of Transverse  
Flowing Particles**

**BY**

**Michael Thomas**

ABSTRACT OF THESIS

Submitted in Partial Fulfillment of the  
Requirements for the Degree of

**Master of Science**

**Electrical Engineering**

The University of New Mexico  
Albuquerque, New Mexico

**July, 2011**

**Iterative Model and Data Analysis for the Estimation of Transverse Flowing  
Particles**

by

**Michael Thomas**

**B.S., Electrical Engineering, New Mexico State University, 2007**

**ABSTRACT**

In traditional flow cytometry, a hydrodynamic sheath is used to precisely position particles for analysis by a tightly focused laser. This precise analysis provides for well-behaved pulse shapes that allow for accurate correlation of scatter and fluorescence pulse width, area, and peak values to particle composition, size, and labeling levels. However, use of hydrodynamic focusing requires purified water and accelerating particles to high linear velocities, both of which dramatically increase the cost of flow cytometry. Several instruments use sheathless approaches to minimize these effects and have proposed differing methods to correct for artifacts caused by unfocused particles traversing less than optimal paths through the interrogation laser. However, no model yet has used a complete physical simulation to provide a predictive model that can be used to determine key pulse shape effects that would be valuable to determine the shape and size of particles passing through the laser beam. Such a model would be useful for both sheathless cytometers and for cytometers that analyze non-traditional particles that are either difficult to focus (very large particles) or have unique shapes.

In order to model the signals generated from unfocused flowing particles traversing a laser, algorithms for different shape geometries must be developed so that the intensity of the Gaussian electric field can be calculated for every detectable position of

the object in question. We have developed algorithms to model both focused and unfocused particles in a Gaussian beam in a variety of shape geometries. Geometries that have been modeled include: Planar objects, sphere- shaped objects to represent beads and eukaryotic cells, and oblong or rod-shaped objects to represent bacterial cells. Included in each algorithm is a scattering efficiency function to more accurately position the object in reference to orthogonal detection. Finally, using linear regression analysis, we have confirmed that the numerical distribution of the physical model generates a Gaussian distribution as expected.



## TABLE OF CONTENTS

<i>LIST OF FIGURES</i> .....	<i>xi</i>
<i>CHAPTER 1 INTRODUCTION</i> .....	<i>1</i>
<i>INTRODUCTION</i> .....	<i>1</i>
<i>BACKGROUND</i> .....	<i>3</i>
<i>TRADITIONAL FLOW CYTOMETRY AND ITS DRAWBACKS</i> .....	<i>6</i>
<i>GAUSSIAN OPTICS</i> .....	<i>7</i>
<i>PULSE SHAPE GENERATION</i> .....	<i>9</i>
<i>CHAPTER 2 GOALS OF WORK</i> .....	<i>10</i>
<i>IMPROVEMENT OF TRADITIONAL FLOW CYTOMETRY</i> .....	<i>10</i>
<i>DEVELOPMENT OF DATA ANALYSIS</i> .....	<i>10</i>
<i>CHAPTER 3 METHODS AND DEVELOPMENT</i> .....	<i>12</i>
<i>FLOW OF DEVELOPMENT</i> .....	<i>12</i>
<i>CALCULATION OF GAUSSIAN ELECTRIC FIELD (GEF)</i> .....	<i>13</i>
<i>PHYSICAL MODEL</i> .....	<i>15</i>
<i>GEOMETRY MODELS AND GENERATION</i> .....	<i>16</i>
<i>SIDE-SCATTER DETECTION</i> .....	<i>20</i>
<i>PULSE GENERATION</i> .....	<i>12</i>
<i>CHAPTER 4 DATA COLLECTION</i> .....	<i>23</i>
<i>INITIAL TESTING: REGRESSION ANALYSIS OF PLANAR MODELS</i> .....	<i>23</i>

<i>COMPARATIVE SHAPE ANALYSIS OF CONCENTRIC RING ARRAY MODELS.....</i>	<i>24</i>
<i>CHAPTER 5 DISCUSSION .....</i>	<i>29</i>
<i>REFERENCES .....</i>	<i>30</i>
<i>APPENDICES</i>	
<i>APPENDIX A - SELECTED SOURCE CODE .....</i>	<i>32</i>

## LIST OF FIGURES

<i>FIGURE 1 FLUIDICS AND OPTICS OF A TYPICAL FLOW CYTOMETER.....</i>	<i>2</i>
<i>FIGURE 2 GENERAL FLOW OF ELECTRONICS AND ANALYSIS OF A MODERN FLOW CYTOMETER.....</i>	<i>6</i>
<i>FIGURE 3 INTENSITY OF COMPLEX GAUSSIAN ELECTRIC FIELD.....</i>	<i>8</i>
<i>FIGURE 4 GAUSSIAN DISTRIBUTION.....</i>	<i>9</i>
<i>FIGURE 5 RING AND CONCENTRIC RING ARRAYS.....</i>	<i>13</i>
<i>FIGURE 6 WAVELENGTH, NUMERICAL APERTURE (NA) AND BEAM WAIST.....</i>	<i>14</i>
<i>FIGURE 7 COMPLEX AMPLITUDE OF GAUSSIAN ELECTRIC FIELD DECLARATIONS.....</i>	<i>14</i>
<i>FIGURE 8 COMPLEX AMPLITUDE OF GAUSSIAN ELECTRIC FIELD.....</i>	<i>15</i>
<i>FIGURE 9 ORIENTATION OF PLANAR OBJECT IN REFERENCE TO THE GAUSSIAN WAVEFRONT.....</i>	<i>16</i>
<i>FIGURE 10 RING ARRAY GENERATION.....</i>	<i>19</i>
<i>FIGURE 11 SIDE-SCATTER POINT RESTRICTION.....</i>	<i>21</i>
<i>FIGURE 12 COMPLEX AMPLITUDE OF GAUSSIAN ELECTRICAL FIELD FOR SINGLE RING ARRAY.....</i>	<i>24</i>
<i>FIGURE 13 COMPLEX AMPLITUDE OF GAUSSIAN ELECTRICAL FIELD FOR SPHERICAL OBJECT.....</i>	<i>25</i>
<i>FIGURE 14 COMPLEX AMPLITUDE OF GAUSSIAN ELECTRICAL FIELD FOR ROD OBJECT.....</i>	<i>25</i>
<i>FIGURE 15 COMPLEX AMPLITUDE OF GAUSSIAN ELECTRICAL FIELD FOR OBLONG OBJECT.....</i>	<i>26</i>

*FIGURE 16A-C COMPLEX AMPLITUDE OF GEF FOR PARALLELISM EVENT .....27*

## Chapter 1

### Introduction

#### 1.1 Introduction

Flow cytometry is a technique to rapidly count or analyze organic and inorganic particles by placing them in a fluidic stream and passing the stream through a detection system comprised of both optical and electronic components collect light and will perform data analysis. Medical professionals and research laboratory personnel currently use flow cytometry, where portability, cost and power are not a priority.

A typical flow cytometer generally consists of five primary components, which include a flow cell, light source, detector, and amplification system and data analysis. A traditional flow cell is the flow cytometry component that transports and aligns the sample through the measuring light source. Particles and cells that pass through the light source, e.g., a focused laser, in the microchannel absorb and fluoresce (emit) depending on their chemical composition and the frequency range of the light source. The detectors of flow cytometers are typically positioned to collect scattered fluorescent light from three directions, i.e., light reflected forward, to the side (orthogonal) and backwards. The three detector systems are generally required in order to differentiate between different particle or cell types or particles traveling through the flow cell. The electronics of the flow cytometer allow the analog signal from the detector to be converted into digital

signals to be analyzed. Finally, data analysis is performed using a processing unit. The optics and fluidics of a typical flow cytometer are shown in Figure 1 below.

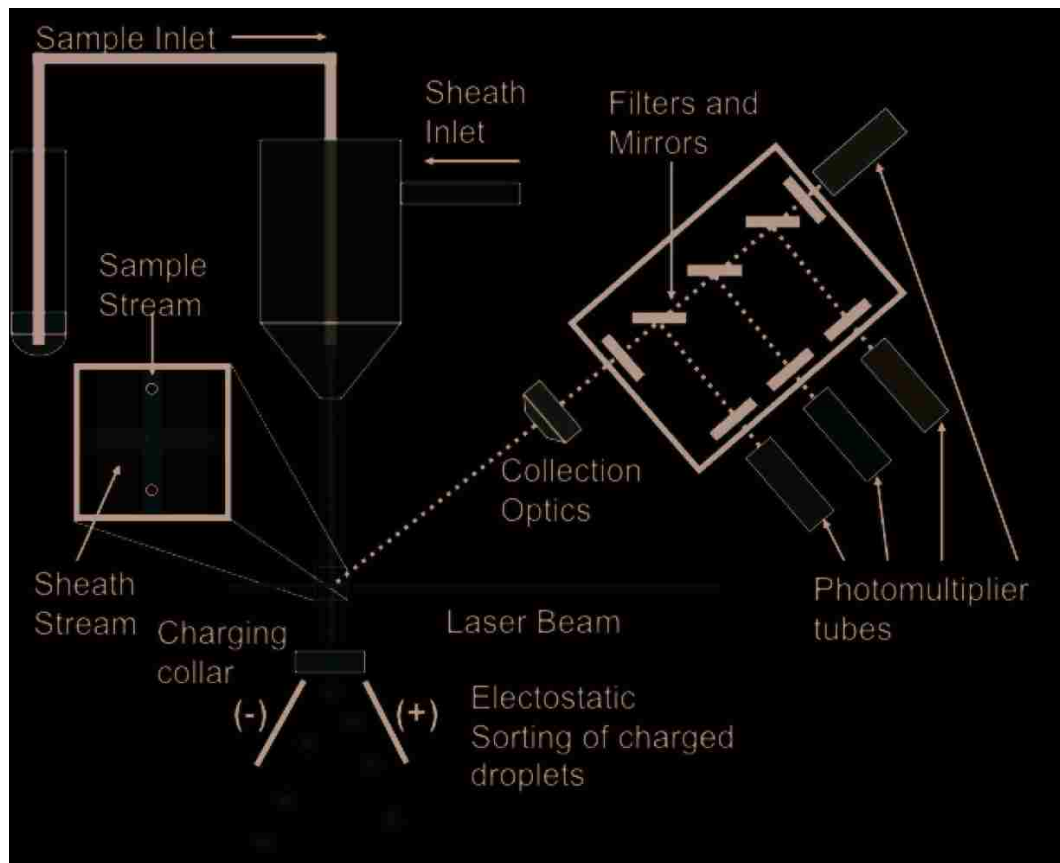


**Figure 1: Typical flow cytometer with light collected across the side-scatter channel. Photomultiplier tubes can be utilized for either light scatter detection or fluorescence detection. In addition, photodiodes can replace photomultiplier tubes for scatter detection along the side scatter channel.**

Typically, analysis includes peak detection and area calculation that is subsequently used in post processing to enable the user to filter or “gate” responses. Note that often the analog-to-digital (ADC) electronics are embedded into the processing unit used for data analysis eliminating the need for separate board level components.

The main contribution of this thesis is the development of acquisition and analysis that support a portable, low cost cytometry instrument. As indicated above, the current

state-of-the-art in flow cytometry instruments is not designed to support portable applications, and as a result, commercial instruments are very expensive and large, stationary pieces of equipment. The development of a portable, low cost instrument can serve multiple applications, in which commercial instruments are not applicable, e.g. field analysis of blood samples from patients in third world countries. In order to reduce cost, the design of several components of existing instruments needs to be re-considered. My specific contributions are to design a data acquisition system and algorithm which may reduce the need of focusing techniques, thus reducing waste of sheath fluid. Additionally, investigation of new signal processing algorithms for extraction of additional information about cell size, shape and chemistry from the digitized signals received by the detectors allow for improvements to the data acquisition present in traditional flow cytometry. The remaining sections of this thesis detail the progress I have made on these goals.

## 1.2 Background

The flow cell of the flow cytometer is a critical component of the flow cytometer. It is vital that there is uniform sensitivity for all detection agents, e.g., side scatter. The authors of previous work have proposed solutions to obtaining such uniformity, which can, for example, be obtained through hydrodynamic focusing. [1] Utilizing hydrodynamic focusing, sheath fluid in combination with specific types of orientations of

nozzles and tubes allow for particles to be aligned into a single path for analysis. In order to achieve hydrodynamic focusing, fluidic velocity of sheath fluid must be approximately 100 times that of the sample. [1,2] In addition to providing hydrodynamic focusing, the flow cell is also designed to remove the unrecyclable sheath fluid or waste. Typically, waste is removed from the flow cell via tubing connected at the bottom of the flow cell.

The type of light source used in flow cytometry varies depending on the application scenario. In this research, a low-power laser light source was chosen to model for several reasons. Low-power lasers provide a flexible wavelength spectrum, while using minimal amounts of energy and keeping costs low, making them ideal for developing low cost devices. [8] Common low-power lasers used in flow cytometry are 488nm, 532nm and 635nm, representing blue green and red light sources respectively. For the detection system, other optical components are required to implement the three detection channels. Such optical components include biconvex lenses to focus light, beam splitters and filters to re-direct light towards detections agents.

Photodetectors in flow cytometry are used to measure light intensity. They generate an analog signal that is proportional to the amount of photons collected by the detector. Photodetectors for flow cytometry can be placed into two categories [3]. The first type of photodetectors to be discussed is photodiodes, which are efficient in bright light conditions and can operate with or without a bias. A second type of photodetectors are photomultiplier tubes or PMTs. PMTs are used commonly in fluorescence measurements and in low-lighted conditions, but require an external power source. A significant drawback of PMTs is their sensitivity to noise. PMTs have very large gain, on order with



$10^6$ , which work to amplify noise sources significantly in the analog output signal. Although the noise components can be filtered using signal processing techniques, photodiodes are much cheaper. Given our objectives are to build a low cost system that meets flow cytometry standards in terms of speed, power consumption and accuracy, we opted to use photodiodes in our detection system.

Pre-amplification is a vital component in signal processing in flow cytometry, especially when photodiodes are used for detection. Pre-amplification is used to provide gain to photodiodes. Such filters can be installed in preamplifiers and be matched to expected pulse shapes [4]. Beyond preamplifier devices, operational amplifiers are used to measure flow cytometry parameters and the configuration of the amplifier will differ based on the parameter to be measured. A common operational amplifier design for fluorescence detection for a PMT calculates the average anode current and pulse height. While these two parameters are important components of a cellular analysis, we determined that pulse shape information, which can be obtained from the photodetectors, provides unique opportunities to further improve the analysis result, as I describe in a later section of this thesis.

Modern electronics provide the opportunity to integrate many functions onto a single chip and does so in a cost effective manner. This is particularly true for integrated circuits used in embedded systems, where ADCs, DACs, analog filters, comparators, and amplifiers [5] are incorporated on the same die as the digital post-processing computational elements. We extensively leverage the capabilities provided by modern microelectronics to achieve our primary design objective of building a cost effective,

low-power flow cytometry system, as we describe in the sections that follow. A general flow of the electronics and analysis of a flow cytometry system is described in Figure 2 below.



**Figure 2: General flow of electronics and analysis of a modern flow cytometer**

### 1.3 Traditional Flow Cytometry and its drawbacks

While the typical and traditional flow cytometry setup as described in the background is fairly robust, there are a few shortcomings in concept and design. For example, relying on hydrodynamic focusing and sheath fluid for uniformity in the flow cell is not always practical due to the large amounts of waste generated from the sheath fluid. A more practical and cost effective approach to achieve uniformity for detection can be an alternative focusing method such as acoustic, dielectrophoretic or hydrodynamic focusing. [2,9,10] Alternatively, a process can be developed in place of focusing techniques where data can be collected from the sample stream without the requirement of a focused path. In developing such a process, maintenance is minimal due to fewer hardware requirements, cost is minimized and waste is reduced eliminating the need for sheath fluid for hydrodynamic focusing.

### 1.3 Gaussian Optics

In this section of the thesis, the theories and concepts of Gaussian beams, Gaussian electric fields and Gaussian probability density functions will be discussed. A Gaussian beam is a Gaussian distribution and function describes an optical beam with an electrical field with amplitude. Complex amplitude of the Gaussian electric field is described in Equation 2, where the complex amplitude of the Gaussian electric field is represented by  $U(r)$ , followed by the complex envelope,  $A(r)$ . The product of  $A(r)$  and a paraxial wave function gives the final  $U(R)$  value.  $U(r)$  is defined in Equation 2.  $A(r)$  must first satisfy the

$$U(r) = A(r)e^{-jkz} \quad (2)$$

paraxial form of the Helmholtz equation as shown in Equation 3. A solution for

$$\nabla_T^2 A - j2k \frac{\partial A}{\partial z} = 0 \quad (3)$$

the paraxial form of the Helmholtz is showing in Equation 4. This solution

$$A(r) = \frac{A_1}{z} e^{-jk \frac{\rho^2}{2q(z)}}, q(z) = z - \epsilon \quad (4)$$

provides a solution to  $A(r)$  and a parabolic wave and a shift,  $\epsilon = jz_0$ . A final expression of  $U(r)$  is defined by Equation 5 and followed by functions, constant

$$U(r) = A_0 \frac{W_0}{W(z)} e^{\left[\frac{\rho^2}{W^2(z)}\right]} e^{\left[-jkz - jk \frac{\rho^2}{2R(z)} + j\zeta(z)\right]} \quad (5)$$

and parabolic wave,  $W(z)$ ,  $R(z)$ ,  $\zeta(z)$ , and  $W_0$  are defined in Equations 6-10.

$$W(z) = W_0 \left[ 1 + \left( \frac{z}{z_0} \right)^2 \right]^{\frac{1}{2}}, \quad \text{spot size} \quad (6)$$

$$R(z) = z \left[ 1 + \left( \frac{z_0}{z} \right)^2 \right], \text{wavefront radius of curvature} \quad (7)$$

$$\zeta(z) = \tan^{-1} \frac{z}{z_0}, \text{Gouy phase shift} \quad (8)$$

$$W(0) = W_0 = \left( \frac{\lambda z_0}{\pi} \right)^{\frac{1}{2}}, \text{waist size} \quad (9)$$

$$p^2 = x^2 + y^2, \text{parabolic wave} \quad (10)$$

[11]

Figure 3 below shows a rendered Gaussian Electric Field for a given laser beam with a wavelength of 532nm.

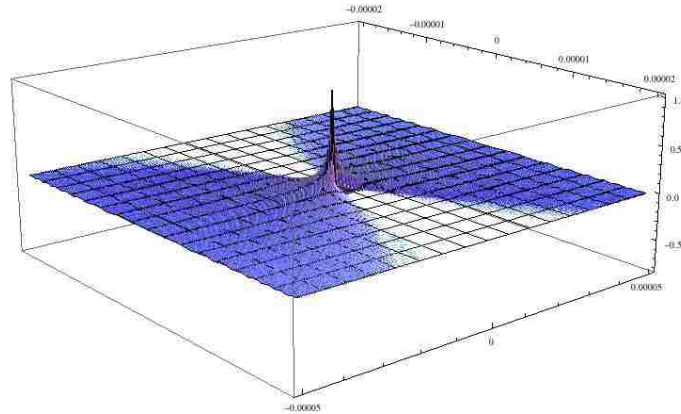


**Figure 3: Complex Gaussian Electric Field of a laser beam with a wavelength of 532nm**

A Gaussian profile can be approximated by Gaussian functions because of the Gaussian profile it emits. Curve fitting techniques can be used to confirm a Gaussian profile and approximate object size and shape based on the components of the Gaussian probability function. A Gaussian Probability Density Function (PDF) can be approximated with a mean,  $\mu$  and the standard deviation,  $\sigma$ . Equation 11 represents the

$$f(x) = \frac{1}{\sqrt{2\pi\sigma^2}} e^{-\frac{(x-\mu)^2}{2\sigma^2}} \quad (11)$$

Gaussian PDF and Figure 1 represents a plot of a Gaussian PDF with a mean of 0 and standard deviation of 1.

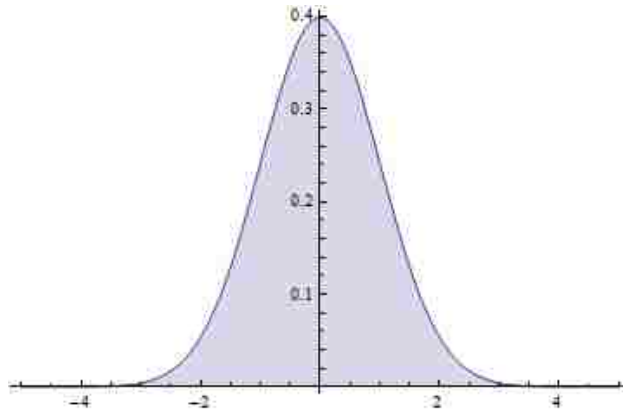


**Figure 4: Gaussian distribution**

#### 1.4 Pulse Shape Generation

As discussed previously, traditional flow cytometry generally collects a peak intensity, area and width values and average current from the detection amplifier circuitry. While these values are adequate for event counts, they do not provide valuable information for differentiating between different particle or cell types in a sample to be analyzed in a flow cell. If peak intensity is incrementally calculated as an object passes through the Gaussian beam, one can generate a full pulse. A generated pulse shape is valuable in the analysis of samples to differentiate between size, shape and other interesting properties. Pulse shape offers a greater amount of valuable information in comparison to traditional data analysis in flow cytometry (e.g. peak intensity and area) and offers potential in analysis for a variety of properties. [12,13]

## Chapter 2

### Goals of Work

#### 2.1 Improvement of Traditional Flow Cytometry

Improvements to current flow cytometry instrumentation can give an ability to provide detection in a flow cell without a focused stream. Traditional flow cytometry requires a focusing technique (e.g. hydrodynamic). Any focusing method generates additional expense for maintenance, and focusing methods such as hydrodynamic focusing produce undesirable waste (e.g. sheath fluid) in order to focus a sample stream. A goal of this research is to provide analysis of a unfocussed sample stream. If this goal can be achieved, we can reduce the hardware required for flow cytometers, reducing maintenance for flow cytometers and eliminating waste generated by sheath fluid if hydrodynamic focusing is being utilizing to focus the sample stream. Finally, advanced instrumentation can allow us to detect parallel or doublet events.

#### 2.2 Development of Data Analysis

A foundation for pulse generation and instrumentation can be based on the calculation of the complex amplitude of the Gaussian Electric Field (GEF) as discussed in the background of this thesis. Developing a model of the complex amplitude of the GEF

allows pulse generation to be possible. By developing a model for the GEF, simulations can be performed in which objects are passed through the given Gaussian beam and a pulse generated. Validation of a generated pulse can be performed by regression analysis to determine whether the generated pulse contains properties of the expected Gaussian distribution. Validation of pulse generation in addition to calculation of the complex amplitude of the Gaussian Electric Field will be described in sections to follow.

## Chapter 3

### Methods and Development

#### 3.1 Flow of Development

I chose Mathematica 7 to perform all calculations of complex amplitude of the Gaussian Electric Field (GEF), geometric shape generations, pulse shape generations, and statistical calculations. The calculation of the amplitude of the GEF (as discussed in 1.3) requires user-defined variables including wavelength, numerical aperture (NA) and beam waist ( $\omega_0$ ). The GEF model returns a three-dimensional function representing the amplitude of the electric field of the beam to be analyzed. This function allows any three-dimensional coordinate to be expressed in the function in order to calculate the GEF amplitude at that individual position in space.

All geometrical models are based on planar models, where all shapes are comprised of individual points in space. A plane is defined, as a two-dimensional space comprised of two or more vectors. These planes a two-dimensional (y,z) objects that are incrementally passed through the beam across the x-axis. In simplest form, more complicated geometries such as a sphere are adjacent planes to represent that three-dimensional geometry. All sphere-based geometries are based on the concentric ring array concept as portrayed in Figure 5. A ring array is a planar array with elements lying on a circle. If several of these arrays with different radii share a



common center, then the resulting planar array is known as a concentric ring array.

[6] Methodology for developing spherical geometries using concentric rings will

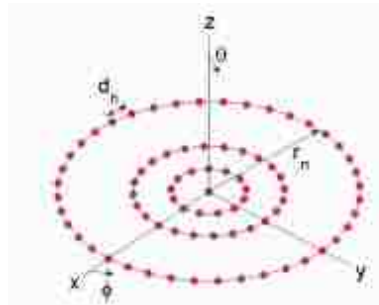


Figure 5: Ring and Concentric Ring Arrays [6]

be discussed later on in this chapter. As each point of each plane has a three-dimensional coordinate to represent its position in space, the GEF amplitude of each position of a plane or geometrical shape can be calculated. However, since multiple points in space are being considered, a summation of GEF amplitudes for each must be calculated in order to determine the overall amplitude of a given object passing through the Gaussian beam. Data analysis was performed in Matlab using the EasyFit toolbox. Data Analysis is discussed later in this chapter.

### 3.2 Calculation of Gaussian Electric Field (GEF)

The function of the Gaussian Electric Field derived in 1.3 must be expressed in code in order to integrate it into the model and evaluate complex amplitude at any given position in space. Initially, there are user-defined constants important to the

model that includes the wavelength of the light source and the numerical aperture of the light collection. In addition, a simple calculation of the beam waist is performed using these two user-defined constants. The wavelength, NA and beam waste as defined in code are shown in Figure 6. A 532nm light source and NA of .6 is used for

$$\begin{aligned} \lambda &= 532 \cdot 10^{-9}; \\ NA &= .6; \\ \omega_0 &= \left( \frac{.65 \lambda}{NA} \right) \left( \frac{1}{2} \right); \end{aligned}$$

**Figure 6: Representation of wavelength, Numerical Aperture (NA) and beam waist in calculation of Gaussian Electric Field**

all calculations in this study. Following these declarations, the definitions for wave front radius of curvature ( $R(z)$ ), beam width ( $W(z)$ ), Guoy phase shift ( $\zeta(z)$ ), and origin of z-axis in accordance to beam waist ( $z_0$ ). The definition of these functions as expressed in code can be seen in Figure 7. Finally, a function representing the

$$\begin{aligned} R2[z_] &:= z \left( 1 + \left( \frac{z_0}{z} \right)^2 \right); \\ \zeta2[z_] &:= \text{ArcTan} \left[ \frac{z}{z_0} \right]; \\ \omega[z_] &:= \omega_0 \sqrt{1 + \left( \frac{z}{z_0} \right)^2}; \\ z_0 &= \frac{\pi \omega_0^2}{\lambda}; \end{aligned}$$

**Figure 7: Declarations in code for the calculation of the complex amplitude of the Gaussian Electric Field**  
 complex amplitude of the Gaussian Electric Field can be expressed after defining the required expressions and constants. A complex function with respect to all three axes

can allow observation of the complex amplitude at any given point in three-dimensional space in order to generate the desired pulse shape. Code expression for the complex amplitude for the GEF as discussed in 1.3 is shown in Figure 8.

$$\mathbf{Efield}[x_, y_, z_] := \frac{\omega_0}{\omega[z]} e^{-\frac{(x^2 + y^2)}{w[z]^2}} e^{-ikz - ik \frac{(x^2 + y^2)}{2R2[z]} + i\phi2[z]};$$

Figure 8: Complex amplitude for the Gaussian Electric Field with respect to the x, y and z axes

### 3.3 Physical Model

As a 532nm green laser is being modeled for all simulations, it is important to consider a beam spot size for reference to objects passing through a given beam. Referring back to Equation 6, spot size can be calculated for a green laser of 543nm. Equation 6 is shown below.

$$\omega(z) = \omega_0 \sqrt{1 + \left(\frac{z}{z_0}\right)^2} \quad (6)$$

[11]

As calculated above, the spot size for the given green laser is approximately  $1.729\mu\text{m}$ . As mentioned previously, all objects modeled in discussed experiments are based on planar models. Any plane or planar slice is passed through a Gaussian beam parallel to

the Gaussian wavefront with respect to the x and z axes. Figure 9 below demonstrates the orientation of a rectangular plane in reference to a Gaussian wavefront.

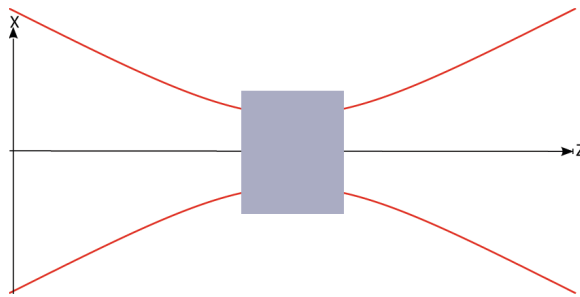


**Figure 9: Orientation of a planar object in reference to the Gaussian wavefront**

### 3.3 Geometry models and generation

All geometric models in this research are in a two-dimensional plane or slices of two-dimensional planar space in order to generate a third dimension. Two-dimensional planar objects are used as a basis for any geometric model simulated in this research. A planar surface can be defined simply as three or more Cartesian points in a two-dimensional space. Initially, simple two-dimensional planes were used to test the calculation of the complex amplitude of the Gaussian Electric Field. The two-dimensional plane used for these tests are in the form of a square or rectangular grid. In order to calculate the complex amplitude of the Gaussian Electric Field of an array of coordinates generating a two-dimensional plane, the summation of the

complex amplitude of the GEF represents the complex amplitude of the entire object in simulation.

When considering a two-dimensional plane in calculation of complex amplitude, all three dimensions must be considered in model development. In the case a simple two-dimensional grid plane, a triple for-loop structure is used to assign three-dimensional Cartesian coordinates. The primary loop assigning the z coordinates as the object passes through the beam and the remaining for loops assign the x and y coordinates, assigning the points of the actual plane. Refer to Appendix A for code of three for loops that assign Cartesian coordinates as a two-dimensional plane passes through the indicated beam. In addition to complex amplitude for the Gaussian Electric Field, a summation of the complex amplitudes must be considered before the object changes the position in the z-axis.

As previously mentioned, three-dimensional shapes to be modeled include spheres, oblong shapes and rods. Spherically based shapes can be represented by slices of two-dimensional planes forming a system of concentric ring arrays. The concept of the concentric ring adds the additional dimension to the geometry required to model a shape such as a sphere. An initial step to creating concentric rings for a sphere or shapes based on spheres is to alter a grid two-dimensional plane to an approximate circular plane. A radius of the circle and thus the sphere and density are user defined for modeling of a circular plane and all shapes based on this plane. Density defined by the user represents the distance between planar points to be generated. Refer to Appendix A for source code to generate a ring array. In simplest

form, initially points are generated from  $(0,r)$  and  $(0,-r)$ . However, since side scatter detection is being simulated, the only geometry of the objects within line of sights of a detector needs to be generated. This concept will be discussed further in section 3.4. For now, discussion will be will not consider side scatter and assume all light is captured.

A single ring is generated with initial points at  $(0,r)$  and  $(0,-r)$  and continues along the perimeter by subtracting a value of “iter” from  $r$  or adding that value to  $-r$ . The value of iter is derived from the density value defined by the user. For example, if a density of 100 is defined, there will be 100 points along the perimeter of a ring from  $(0,r)$  or  $(0,-r)$  to the approximate point of  $(r,0)$ . If all light collection is to be considered, the negative portion of the  $y$ -axis needs to be generated as well. Figure 10 is a description of a ring array where points are generated in the positive  $y$ -axis. A concentric ring array allows for the third dimension to be modeled for objects such as spheres.

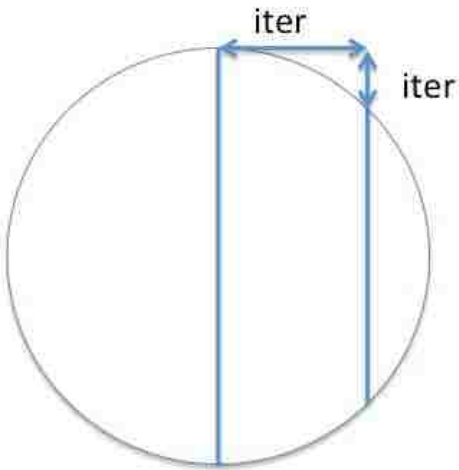


**Figure 10: Ring array point generation with iter value**

Similar to points along the perimeter of a single ring, one can adjust the radii of a ring using the same “iter” value as desired.

As discussed previously, spheres, rods and oblong shapes were to be modeled in these experiments. All of these geometric shapes can be generated using the discussed techniques of concentric rings. A rod, unlike a sphere has a defined length that has consistent radii where rings can be identical with just an offset in the z-axis. The remaining geometry can be generated just as the sphere was and was described previously in this section. Oblong objects are modeled similarly to a sphere with a single exception, where an oblong object is asymmetrical. In the development of a geometrical model for an oblong object, a single axis must be defined as asymmetrical. To create a non-symmetrical axis in a ring array, slope is to be adjusted by applying a given scale to the value of “iter”.

As previously mentioned, a goal in this research is to reduce waste of sheath fluid to increase portability. As a result parallelism of particles travel through the flow cell causing difficulties to differentiate between different events without a traditional focused sample stream. However, while events not in a focused sample stream makes accurate detection more difficult, a faster flow rate can be achieved using parallelism. Refer to Figure 6 in section 2.1 for an example of parallelism where objects are offset. In my research I have modeled parallelism or doublet events where objects are in parallel of each other as they pass through the low power laser light source. When simulating objects in parallelism, each object is simulated individually at their defined physical position.

#### 3.4 Side-scatter Detection

As mentioned in 3.3, the method and model used to generate the geometry considered that all light was captured. If a flow cytometry system is to be modeled, detection schemes need to be modeled as well. As mentioned in section 1.1, flow cytometry detection can include forward, back, and side scatter detection. However, because this simulation is in early development, only side or orthogonal scatter detection is being considered. Due to the orthogonally of the detector, only the portion of an individual ring that is within line of sight of the detector will be detected. Therefore, instead of generating points for an entire object, it is only required to do so for portions of the object that is detected. In modeling concentric



rings in side-scatter detection, detection is available between 0 and  $\frac{\pi}{2}$  or 0 and 45 degrees. However, detection does not occur at exactly 0 and  $\frac{\pi}{2}$  or 0 and 45 degrees.

Figure 8 describes code that restricts points to the detected region.

```
NumA = .6;  
If[k = 1, y = 0  
    theta = 0];  
If[k > 1 && k < 52,  
    theta = (k - 1) 0.9];  
If[k = 51, theta = 45];  
If[k > 51 && k < 101,  
    theta = 45 - (k - 51) 0.9];  
y = y + iter;  
    theta  
effrat =  $\frac{\theta}{45}$ ;  
eff = NumA effrat;
```

Figure 11: Source code to restrict generated points to only the region detected by side scatter

An additional consideration of detection to consider is the efficiency or amount of light to be collected. Numerical aperture (NA) is the range of angles in which a given optical system can collect light. [7] A numerical aperture of 0.6 is assumed for all simulations. The numerical aperture is represented in simulation as an efficiency function, “eff”. The product of this efficiency function “eff” and any complex amplitude is calculated to ensure only collected light is to be simulated for analysis. While the NA value of 0.6 is used for all simulations, it is a user defined value and can be adjusted if desired.

### 3.5 Pulse Generation

As discussed in section 1.4, a vital component of flow cytometry instrumentation is generate a pulse representing all detected light as an object passes through the given Gaussian light source. To generate a pulse representing an object event, any complex amplitude or summation of complex amplitudes at position  $(x,y,z)$  must be saved into memory. For simplicity, a log file was generated that included a z-axis position in the Gaussian light source and the complex amplitude at that given position. The generated log file can be imported into the third party software to plot and analyze the generated pulse. Such third party packages used for analysis in this study was Matlab. Refer to Chapter 4 for further discussion on data analysis.

## Chapter 4

### Data Analysis and Results

#### 4.1 Initial Testing: Regression Analysis of Planar Models

As discussed in 3.3, two-dimensional planar models are a basis for ring arrays, concentric ring arrays and thus give the ability to model three-dimensional objects such as a sphere. Using a Matlab toolbox, EasyFit, regression analysis can be performed. As discussed previously, the probability density function of any object traveling through a Gaussian beam, can be approximated by the probability density function of the Gaussian distribution. Therefore, using a regression tool such as EasyFit, we can confirm the validity of the calculation of the complex amplitude of the Gaussian Electric Field. If the data returned by simulation can be fit to the Gaussian distribution, then an experiment is valid. Initially, a planar grid was to be validated in order to implement any planar model for ring arrays and concentric ring arrays. After validation of a planar grid, a ring array was to be analyzed so that models based on concentric ring arrays could be developed. Figure 9 shows a regression plot of a ring array of with a density of 100 (discussed in 3.3) and evaluated across 100 positions across the z-axis.

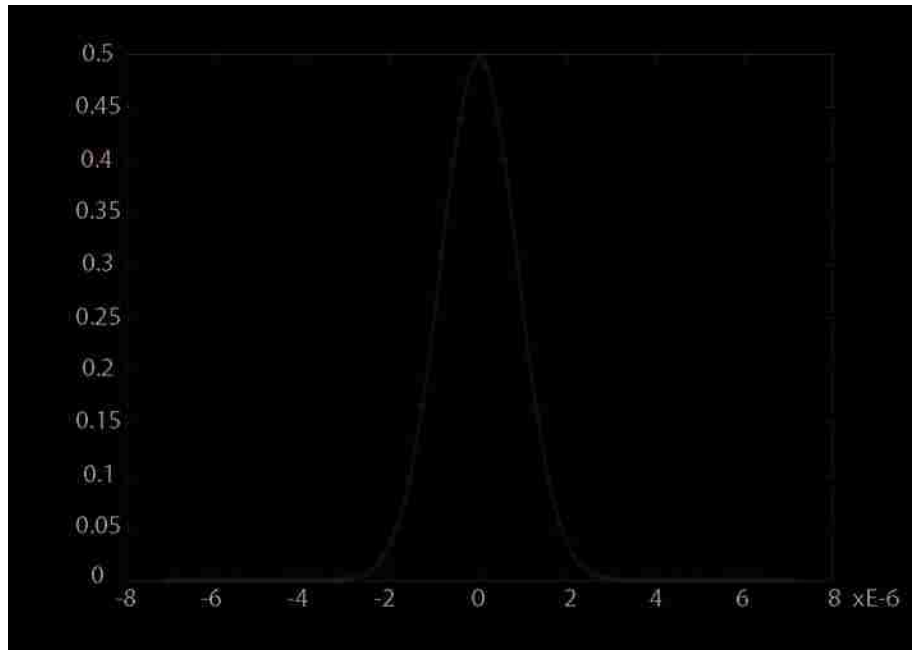


**Figure 12: Complex Amplitude of GEF for single ring array. Complex peak amplitude of 0.49538**

#### 4.2 Comparative Shape Analysis of Concentric Ring Array Models

After validation of a planar grid and ring array, the complex objects based on concentric ring arrays were to be validated by the same technique. Objects to be validated based on concentric ring arrays are a sphere, rod and oblong object. All simulations were performed with a density of 100 across 100 samples along the axis. The regression analysis for the sphere, rod and oblong objects are shown in figures 10, 11 and 12 respectively.

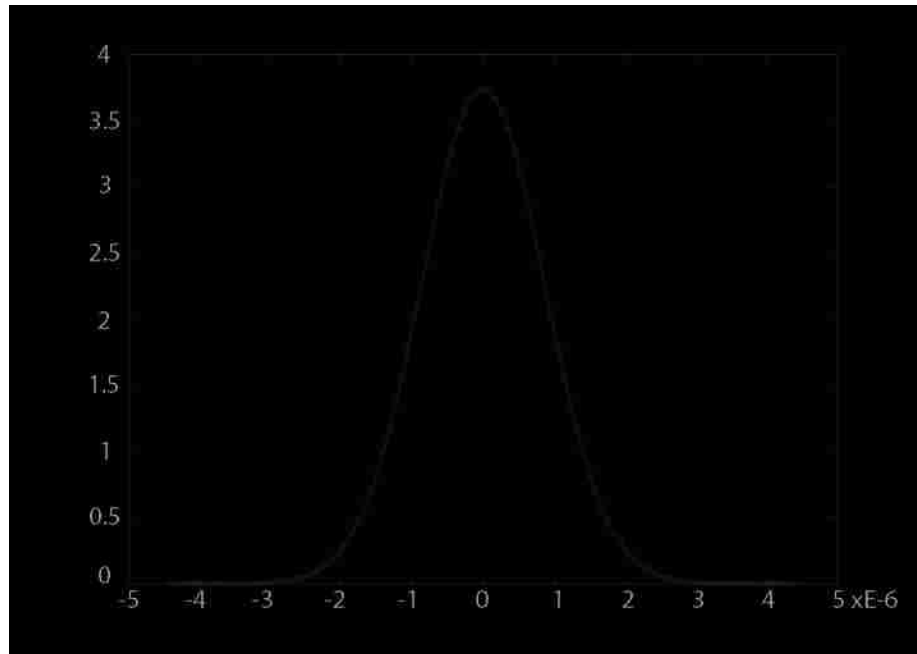


**Figure 13: Complex Amplitude of GEF for spherical object. Complex peak amplitude of 3.7353**

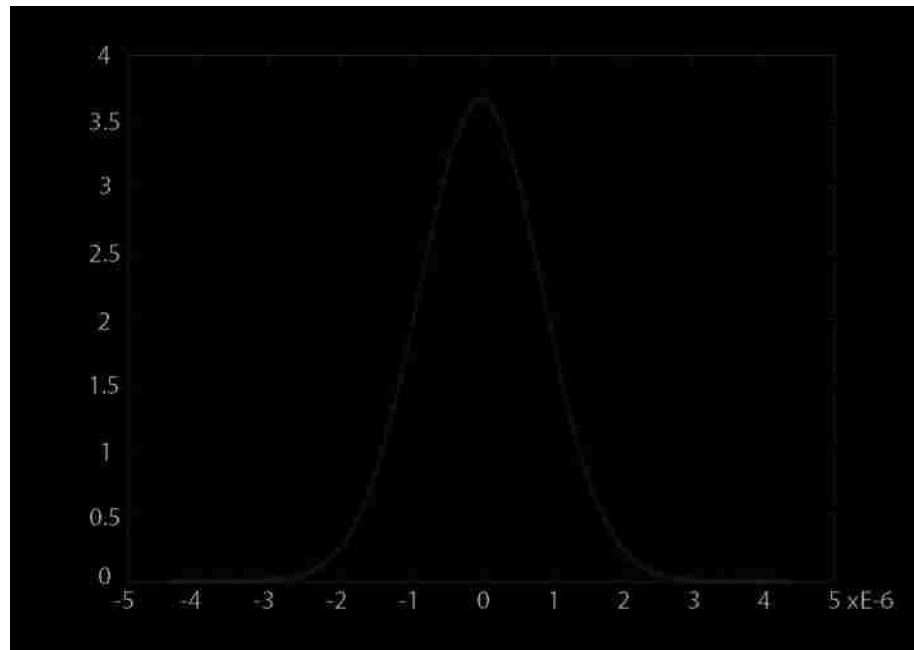


**Figure 14: Complex Amplitude of GEF for rod shaped object. Complex peak amplitude of 3.6633**

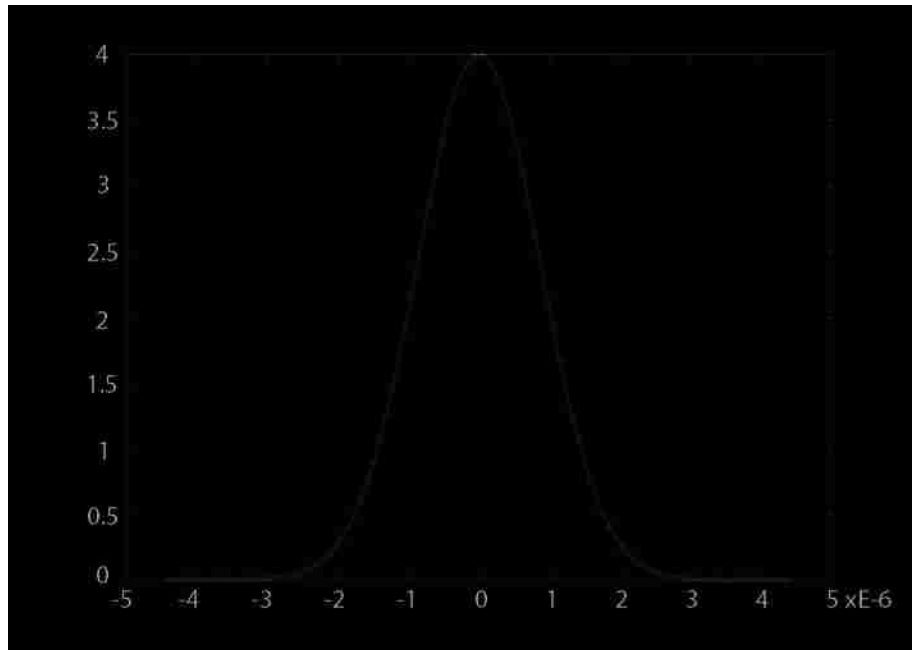


**Figure 15: Complex Amplitude of GEF for oblong object. Complex peak amplitude of 3.991**

In addition to validation of individual objects of spheres, rods and oblong shapes, two spheres in a parallel orientation were modeled and data was collected. This is a very important experiment to perform due to the goal of increased portability by reducing waste. In doing so, the current technique being analyzed to do so is to eliminate hydrodynamic focusing thus creating parallel events. Analysis of events in multiple flow paths is a necessity to achieve the goal of portability. Figure 13 a, b and c graphically describe the total complex amplitude of two identical spheres, a and b are traveling through a Gaussian beam in parallel.

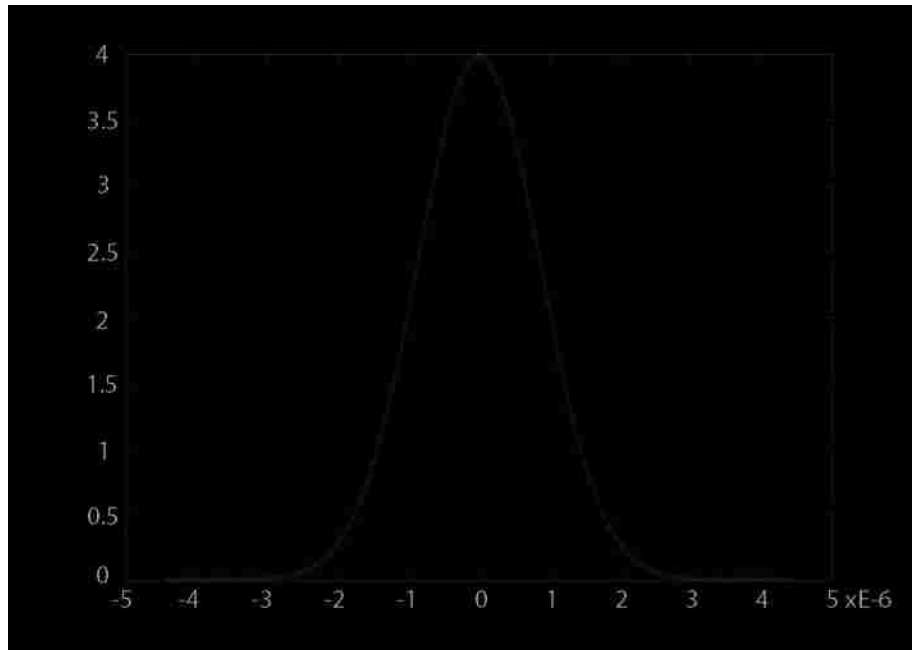


**Figure 16a: Complex Amplitude of GEF for identical sphere a. Complex peak amplitude of 3.9849**

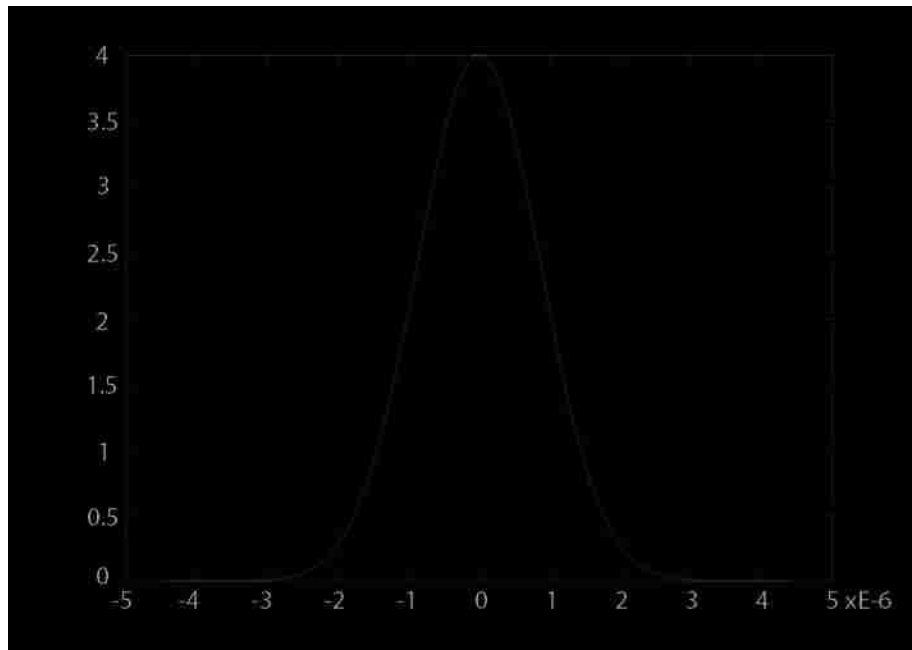


**Figure 16b: Complex Amplitude of GEF for identical sphere b. Complex peak amplitude of 3.9985**

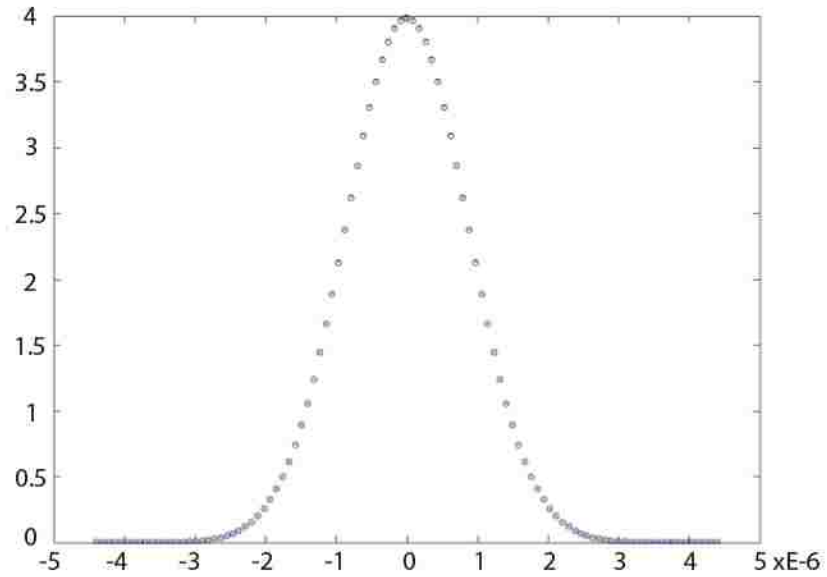


**Figure 16c: Comparison of complex amplitude of GEF for identical spheres a (o) and b (x)**

Unfortunately, because separate waveforms cannot be generated at this time, we must rely on the value of the peak complex amplitude in comparison to a single sphere of the same size in order to determine if there is a doublet event.

Primarily, peak amplitude can determine the differentiation between shape and size of objects passing through the Gaussian beam. Due to time constraints, a study was not performed for each object based on size.



## Chapter 5

### Discussion

As the need for more portable, affordable and efficient flow cytometers grows, the need for development to find solutions to meet these goals will increase. The steps taken described in this thesis have taken steps towards these goals. In many ways, when portability is achieved, so is affordability. We are striving to use cost efficient parts as well reduce constant maintenance and materials in the form of sheath fluid. In removing the sheath fluid, a faster flow rate can be achieved creating more efficient devices. Efficiency can also be achieved by improving the current standard of flow cytometry instrumentation where in general peak intensity and area is being calculated, instead of waveforms where a greater deal of knowledge about a sample can be achieved.

While the research conducted in this thesis was limited to shape differentiation and parallels detection primarily by complex amplitude, it is a primer for analysis to determine shape, size and other property differences by pulse shape in addition to intensity. Future research will be exciting for the development of low cost portable flow cytometry systems and the potential they possess as alternatives to the expensive, stationary devices that are standard today.

## References

- [1] Reynolds, O. (1883). An experimental investigation of the circumstances which determine whether the motion of water shall be direct or sinuous, and the law of resistance of parallel channels. Philos. Trans. Roy. Soc. 174, pp. 935-982. London.
- [2] Van Dilla, M. A., Dean, P. A., Laerum, O. U., Melamed, M. R., (1985). Flow Cytometry: Instrumentation and Data Analysis. Academic Press, London.
- [3] Hiebert, R. D. (1979). Light sources, detectors and flow chambers. In “Flow Cytometry and Sorting” (M.R. Melamed, et al). pp. 623-637. Wiley, New York.
- [4] Shapiro, H. M., Schildkraut, E. R., (1979) The Block Engineering Cytomat-R system. In “Flow Cytometry and Sorting” (M.R. Melamed, et al). pp. 623-637. Wiley, New York.
- [5] Preydko M. (2008). Programming and Customizing the PIC Microcontroller. McGraw-Hill Companies Inc, New York.
- [6] Haupt, R. L., Thinned concentric ring array. *Proc. IEEE Antennas Propagation Int. Symp.*, 1-4, 2008.
- [7] Greivenkamp, J. E., (2004). Field Guide to Geometrical Optics. SPIE Field Guides vol. FG01.
- [8] Habbersett, R. C., Naivar, M. A., Woods, T. A., Goddard, G. R. and Graves, S. W. (2007), Evaluation of a green laser pointer for flow cytometry. Cytometry Part A, 71A: 809–817.

- [9] Goddard, G.R., Sanders, C.K., Martin, J.C., Kaduchak, G., Graves, S.W. (2007) Analytical Performance of an Ultrasonic Particle Focusing Flow Cytometer. *Analytical Chemistry*, 79 (22), 8740-8746.
- [10] Fiedler, S., Shirley, S.G., Schnelle, T., Fuhr, G. (1998) Dielectrophoretic Sorting of Particles and Cells in a Microsystem. *Analytical Chemistry*, 70(9), 1909-1915.
- [11] Saleh, B., E., A., Teich, M.C. (1991). *Fundamentals of Photonics*. New York: John Wiley & Sons. Chapter 3, "Beam Optics," pp. 80–107.
- [12] Naivar, M. A., Wilder, M. E., Habbersett, R. C., Woods, T. A., Sebba, D. S., Nolan, J. P. and Graves, S. W. (2009), Development of small and inexpensive digital data acquisition systems using a microcontroller-based approach. *Cytometry Part A*, 75A: 979–989.
- [13] Naivar, M. A., Parson, J. D., Wilder, M. E., Habbersett, R. C., Edwards, B. S., Sklar, L., Nolan, J. P., Graves, S. W., Martin, J. C., Jett, J. H. and Freyer, J. P. (2007), Open, reconfigurable cytometric acquisition system: ORCAS. *Cytometry Part A*, 71A: 915–924.

## Appendix A – Selected Source Code

### I. Declaration

```
Clear["Global`*"]

λ = 532 10-9;
Eo = 1;
NA = .1;
ωo =  $\left(\frac{.65 \lambda}{NA}\right) \left(\frac{1}{2}\right)$ ;
x = -10-4;
y = -10-27;
z = -10-27;
eff = .6;

r = RandomReal $\left[\left\{\frac{1}{2}, .25 \omega_o, .25 \omega_o\right\}\right]$ ;
dens = 100;
n = dens 10;
iter =  $\frac{r}{dens}$ 

k =  $\frac{2 \pi}{\lambda}$ ;

ω[z_] := ωo  $\sqrt{1 + \left(\frac{z}{z_o}\right)^2}$ 

z_o =  $\frac{\pi \omega_o^2}{\lambda}$ ;

R2[z_] := z  $\left(1 + \left(\frac{z_o}{z}\right)^2\right)$ ;

ζ2[z_] := ArcTan $\left[\frac{z}{z_o}\right]$ ;

f =  $\frac{1}{k \omega_o}$ ;
ξ =  $\frac{x}{\omega_o}$ ;
η =  $\frac{y}{\omega_o}$ ;
ζ =  $\frac{z}{2 z_o}$ ;
b =  $\frac{kx}{k}$ ;
c =  $\frac{ky}{k}$ ;
```

## II. Complex Amplitude of GEF

$$\text{simplify}\left[\frac{1}{4\pi f^2} \left( (1-b^2) \hat{x} - b c \hat{y} - \sqrt{(1-b^2-c^2)} \hat{z} \right) e^{-\frac{1}{4f^2} (b^2+c^2) + i \frac{b}{f} \xi + i \frac{c}{f} \eta + i \frac{1}{f^2} \sqrt{(1-b^2-c^2)} \zeta} \right] /. \mathbf{kx} \rightarrow 0 /. \mathbf{ky} \rightarrow 0];$$

`EfieldGeneral = %;`

$$\text{Efield}[\mathbf{x}_-, \mathbf{y}_-, \mathbf{z}_-] := \frac{\omega_0}{\omega[z]} e^{-\frac{(x^2+y^2)}{\omega[z]^2}} e^{-i\mathbf{kz} - i\mathbf{k} \frac{(x^2+y^2)}{2R_2[z]} + i\zeta[z]};$$

`Efield[x, y, z];`

$$\text{Intfxn}[\mathbf{x}_-, \mathbf{y}_-, \mathbf{z}_-] := \text{Efield}[\mathbf{x}, \mathbf{y}, \mathbf{z}] \left( \frac{\omega_0}{\omega[z]} e^{-\frac{(x^2+y^2)}{\omega[z]^2}} e^{i\mathbf{kz} + i\mathbf{k} \frac{(x^2+y^2)}{2R_2[z]} - i\zeta[z]} \right);$$

`Intfxn[x, y, z];`

### III. Ring Array

```

For [i = -2 10-4, i < 2 10-4 + 4 10-7, i = i + 4 10-7,
  For [j = 1, j < n 10-1 + 1, j = j + 1,
    For [k = 1, k < n 10-1 + 1, k = k + 1,
      If [j == 1, y = 0];
      If [j == 1, new = 2 r]
      If [k == 1, z = r];
      z = r - iter;
      If [z == -r, Break[]]];
    y = y + iter;
    new = new - iter;
    intprimesum = intprime;
    intprime = ParallelSubmit[Re[Intfxn[i, y, z] /. xhat -> 1 /. zhat -> 0] eff];
    If [k > 1, sum = intprime + intprimesum, sum = intprime];
    If [new < 1 10-15, Break[]]];
  For [jj = 1, jj < n 10-1 + 1, jj = jj + 1,
    For [kk = 1, kk < n 10-1 + 1, kk = kk + 1,
      If [jj == 1, y = 0];
      If [jj == 1, new = 2 r]
      If [kk == 1, z = r];
      z = r - iter;
      If [z == -r, Break[]]];
    y = y - iter;
    new = new - iter;
    intprime = Re[Intfxn[i, y, z] /. xhat -> 1 /. zhat -> 0] eff;
    If [kk > 1, sum = sum + intprime + intprimesum, sum = intprime]];
  If [sum > 1 10-27, Break[]]
  Print[sum]]];

ival = N[i]
sumval = N[sum]

iiter = N[ $\frac{2 \text{Abs}[ival]}{10}$ ]

```

```

For [i = ival, i < -ival + iiter, i = i + iiter,
  For [j = 1, j < n + 1, j = j + 1,
    For [k = 1, k < n + 1, k = k + 1,
      If [j == 1, y = 0];
      If [j == 1, new = 2 r]
        If [k == 1, z = r];
        z = r - iter;
        If [z == -r, Break[]]];
      y = y + iter;
      new = new - iter;
      Clear [sum, intprimesum, intprime];
      intprimesum = intprime;
      intprime = Re [Intfxn [i, y, z] /. xhat -> 1 /. zhat -> 0] eff ;
      If [k > 1, sum = intprime + intprimesum, sum = intprime];
      If [new < 1 10-15, Break[]]];
  For [jj = 1, jj < n + 1, jj = jj + 1,
    For [kk = 1, kk < n + 1, kk = kk + 1,
      If [jj == 1, y = 0];
      If [jj == 1, new = 2 r];
      If [kk == 1, z = r];
      z = r - iter;
      If [z == -r, Break[]]];
      y = y - iter;
      new = new - iter;
      intprime = Re [Intfxn [i, y, z] /. xhat -> 1 /. zhat -> 0] eff ;
      If [kk > 1, sum = sum + intprime + intprimesum, sum = intprime];
      If [new < 1 10-15, Break[]]];
  If [kk > n - 1, Print [N [i]]]];

```